

Does prey availability influence the detection of *Dinophysis* spp. by the Imaging FlowCytobot?

Emilie Houliez^{1*}, Alexis D. Fischer², Brian D. Bill³, Stephanie K. Moore⁴

1. Fulbright Scholar sponsored by the Franco-American Fulbright Commission and Guest Researcher at the Northwest Fisheries Science Center, National Marine Fisheries Service, National Oceanic and Atmospheric Administration, Seattle, WA, 98112, USA

2. University Corporation for Atmospheric Research, under contract to Northwest Fisheries Science Center, National Marine Fisheries Service, National Oceanic and Atmospheric Administration, Seattle, WA, 98112, USA

3. Environmental and Fisheries Science Division, Northwest Fisheries Science Center, National Marine Fisheries Service, National Oceanic and Atmospheric Administration, Seattle, WA, 98112, USA

4. Conservation Biology Division, Northwest Fisheries Science Center, National Marine Fisheries Service, National Oceanic and Atmospheric Administration, Seattle, WA, 98112, USA

* Corresponding author: emilie.houliez@fulbrightmail.org

1 **Abstract**

2

3 The Imaging FlowCytobot (IFCB) is a field-deployable imaging-in-flow cytometer that is
4 increasingly being used to monitor harmful algae. The IFCB acquires images of suspended
5 particles based on their chlorophyll-*a* fluorescence and/or the amount of light they scatter (side
6 scattering). The present study hypothesized that fluorescence-based image acquisition **would**
7 undercount *Dinophysis* spp., a genus of non-constitutive mixotrophs, when prey is limited. This
8 is because *Dinophysis* spp. acquire plastids via ingestion of their ciliate prey *Mesodinium* spp.,
9 and lose photosynthetic capacity and autofluorescence in the absence of prey. Even small blooms
10 of *Dinophysis* spp. can be highly toxic and result in diarrhetic shellfish poisoning (DSP),
11 highlighting the importance of accurately detecting low abundances. To explore this, laboratory
12 experiments were conducted to determine optimal IFCB settings for a fed culture of *Dinophysis*
13 *acuminata*, and an existing time series of IFCB observations collected in Puget Sound
14 (Washington, U.S.A) was used to compare *Dinophysis* spp. abundance estimates from samples
15 triggered via side scattering versus fluorescence in relation to *Mesodinium* spp. abundance. This
16 study introduces a quantitative approach for optimizing the detection of target harmful algae
17 which can be repeated across multiple IFCBs and demonstrates the effects of IFCB calibration
18 on *Dinophysis* spp. detection. The laboratory experiments showed that IFCB settings for
19 fluorescence-based image acquisition need to be fairly sensitive to accurately detect *D.*
20 *acuminata* cells. A poorly calibrated IFCB can miss a significant proportion of *D. acuminata*
21 abundance whatever the method used to trigger the image acquisition. Field results demonstrated
22 that the physiological status of *Dinophysis* spp. can influence their detection by the IFCB when
23 triggering on fluorescence. This was observed during a 7-day period when the IFCB failed to
24 detect *Dinophysis* spp. cells when triggering on fluorescence while cells were still detected using
25 the side scattering triggering method as well as observed by microscopy. During this period,
26 *Mesodinium* spp. was not detected, IFCB-derived autofluorescence level of individual cells of
27 *Dinophysis* spp. was low, and less than 50% of *Dinophysis* spp. cells exhibited autofluorescence
28 under the microscope. Together, this indicates that the unique feeding ecology of *Dinophysis*
29 spp. may affect their detection by the IFCB when cells are starved.

30

31 **Keywords:** Imaging FlowCytobot, harmful algal bloom, *Dinophysis*, *Mesodinium*, mixotroph

32 ***1. Introduction***

33

34 Harmful algal blooms (HABs) threaten human health and coastal economies through the
35 production of toxins and other bioactive compounds. In marine systems, one of the most
36 effective ways to reduce or eliminate the societal impacts of HABs is to provide early warning
37 (Brown et al. 2012). Adequate early warning enables mitigation strategies to be put into place to
38 prevent human exposures to HAB toxins and minimize economic losses that may be associated
39 with management strategies designed to protect human health (Anderson et al. 2001; Jin and
40 Hoagland 2008). HAB early warning is most often provided through microscopy-based
41 monitoring of the causative organisms that triggers some management response (e.g., toxin
42 testing in shellfish tissues or proactive shellfish harvest closures) when abundance thresholds are
43 exceeded (Belin et al. 2021; Trainer and King 2023; Trainer and Suddleson 2005). However,
44 because traditional microscopy-based monitoring methods are labor intensive, sample collection
45 is often conducted on weekly or biweekly timescales that are not always adequate for detecting
46 rapidly developing HABs. This can shorten the opportunity to provide early warning which
47 increases risk to the public for toxin exposure and/or the likelihood of costly recalls of
48 contaminated shellfish, especially for HABs that cause toxicity at low abundances.

49 Dinoflagellates in the genus *Dinophysis* can produce toxins (collectively called diarrhetic
50 shellfish toxins [DSTs]) that cause the syndrome diarrhetic shellfish poisoning (DSP) in humans
51 (Reguera et al. 2014; Reguera et al. 2012) at low abundances less than ~ 200 cells L^{-1} (Yasumoto
52 et al. 1985). To address this problem, new technologies are increasingly being used to rapidly
53 and autonomously detect developing HABs *in situ* (Anderson et al. 2012; Glibert et al. 2018).

54 One such technology is the Imaging FlowCytobot (IFCB). The IFCB is a field-
55 deployable, imaging-in-flow cytometer that continuously captures high-resolution images of
56 particles taken from aquatic environments. It samples and analyzes nominal 5 mL water samples
57 approximately every 20 minutes, providing valuable data on the size, shape and autofluorescence
58 characteristics of the imaged particles, over deployments that can last up to several months
59 (Olson and Sosik 2007). When the IFCB is paired with a machine learning image classifier, this
60 system can count and identify multiple HAB species and other phytoplankton (between ~10–150
61 micrometers in size) to the genus-level and sometimes species-level with demonstrated accuracy
62 comparable to that of human experts (Sosik and Olson 2007). The IFCB is a powerful tool for
63 advancing early warning of HABs that is rapidly gaining popularity. At the time of this writing, a
64 total of 103 IFCBs are in use worldwide and 53% of them were acquired during the four last
65 years. In California coastal waters, a statewide network of 12 IFCBs is currently being used to
66 implement an automated early warning system for the detection of HABs at 9 critical land-based
67 locations in addition to four research cruises (Kudela et al. 2021; <https://sccoos.org/ifcb/>).

68 A notable example of an IFCB providing HAB early warning is when an IFCB deployed
69 in Port Aransas, Texas detected a *Dinophysis* spp. bloom ahead of the 2008 Rockport Oysterfest
70 – which attracted up to 30,000 people – and prompted alerts to shellfish managers that likely
71 averted an outbreak of DSP (Campbell et al. 2010). While HABs of *Dinophysis* spp. have been
72 documented in Western Europe, Chile, Perú, and Japan since the 1970s (Reguera et al. 2014),
73 they were not known to cause harm in the U.S. until the 2008 event (Anderson et al. 2021). The
74 first conclusive cases of DSP in the U.S. occurred in 2011 when a family was sickened after
75 consuming recreationally harvested mussels from Puget Sound, Washington (Lloyd et al. 2013;
76 Trainer et al. 2013). Today, shellfish harvesting closures due to unsafe levels of DSTs are

77 enforced annually at multiple sites throughout the U.S. and *Dinophysis* spp. are considered an
78 emerging threat (Anderson et al. 2021; Ayache et al. 2023; Hattenrath-Lehmann et al. 2013). In
79 recognition of this, investments have been made to establish a national network of IFCBs to
80 better understand *Dinophysis* spp. HABs and their drivers (NCCOS and US IOOS 2020). With
81 the expanded use of IFCBs to provide early warning of HABs of *Dinophysis* spp., it is becoming
82 increasingly important to identify factors that might affect their performance.

83 The IFCB can be configured to detect particles using side scattering (which depends on
84 the size of the particle) and/or laser-induced chlorophyll-*a* fluorescence. Particle detection using
85 side scattering detects all particles that scatter light, including detritus, the abundance of which
86 generally greatly exceeds that of phytoplankton in coastal systems (Olson and Sosik 2007).
87 Fluorescence-based particle detection only images particles with chlorophyll-*a* and is more often
88 used for HAB (and phytoplankton) monitoring and detection. Different approaches for tuning the
89 IFCB include adjusting settings to image as wide a size range of phytoplankton as possible (e.g.,
90 Neeley et al. 2021), or to maximize detection of target (HAB) species - however, the latter is
91 rarely done in a quantitative way. Non-optimal IFCB settings are likely to undercount target
92 HAB species, thereby compromising the ability of the IFCB to provide early warning of HABs,
93 particularly if mitigation actions depend on species abundances exceeding specified management
94 thresholds.

95 Even with a well-tuned IFCB, fluorescence-based detection of *Dinophysis* spp. may be
96 complicated by its unique feeding ecology. *Dinophysis* spp. are non-constitutive mixotrophs and
97 combine phototrophy and heterotrophy. They lack permanent plastids (chloroplasts) and must
98 acquire them via ingestion of the ciliate *Mesodinium* spp. that itself steals them by feeding on
99 cryptophytes belonging to the *Teleaulax-Plagioselmis-Germinigera* (TPG) clade (Hansen et al.

100 2013; Park et al. 2006; Park et al. 2008). The size of *Mesodinium* spp. and time lag between
101 *Mesodinium* spp. and *Dinophysis* spp. blooms both influence *Dinophysis* spp. physiological
102 status and formation of intense blooms (Harred and Campbell 2014; Smith et al. 2018). Though
103 *Dinophysis* spp. can survive extended periods without prey (up to three months), they must
104 regularly feed to sequester new plastids to maintain optimal growth and their ability to
105 photosynthesize (Kim et al. 2012; Park et al. 2008). In the absence of prey, the photosynthetic
106 capacity and autofluorescence of *Dinophysis* spp. progressively decrease (Park et al. 2008),
107 which could compromise the ability of the IFCB to accurately detect these cells. Despite
108 declining growth rates and photosynthetic capacity, toxin production continues during starvation
109 leading to increased cellular toxicity (García-Portela et al. 2018; Nielsen et al. 2012; Nielsen et
110 al. 2013). Due to the acute health risk posed by starved *Dinophysis* spp cells, it is important to
111 accurately detect cells with reduced autofluorescence.

112 The goal of this study was to determine if the ability of the IFCB to detect *Dinophysis*
113 spp. varies due to different physiological characteristics of cells related to prey availability. It
114 was hypothesized that the IFCB fluorescence-based image acquisition would undercount
115 *Dinophysis* spp. cells exhibiting weak autofluorescence when prey is limited. To explore this,
116 laboratory experiments were conducted to determine optimal settings of the IFCB for a culture of
117 *Dinophysis acuminata*, and an existing time series of IFCB observations collected in Puget
118 Sound was used to compare *Dinophysis* spp. abundance estimates from samples triggered via
119 side scattering and fluorescence in relation to *Mesodinium* spp. abundance.

120

121

122 2. *Materials and methods*

123 2.1. *Optimization of IFCB settings*

124
125 Laboratory experiments were conducted to identify the optimal IFCB configuration
126 settings for detecting *Dinophysis* spp. and to assess the adequacy of IFCB settings used to obtain
127 the existing time series in Puget Sound. Both time series and laboratory measurements were
128 collected with the same IFCB. *D. acuminata* was chosen for the experiment because it is
129 commonly found in Puget Sound (Ayache et al. 2023; Trainer et al. 2013). However, because no
130 established cultures of local strains of *D. acuminata* were available, the experiments were
131 conducted using the DANY1 strain isolated from the Peconic Estuary, Long Island Sound, NY in
132 May 2013. *D. acuminata* was maintained under favorable growth conditions following the
133 methodology of Park et al. (2006) using the ciliate *Mesodinium rubrum* as prey. *D. acuminata*
134 was grown in 0.22 μm filtered natural seawater (salinity 25, 18°C) and fed twice a week with a
135 Japanese strain of *M. rubrum* (JAMR). *M. rubrum* was grown in F/6-Si (salinity 25, 15°C) and
136 was fed once a week with a Japanese strain of the cryptophyte *Teleaulax amphioxeia* (JATA)
137 that was grown in L1-Si (salinity 22, 18°C). All cultures were grown under white light of ~ 100
138 $\mu\text{mol photons m}^{-2} \text{ s}^{-1}$ intensity and with a 12:12 light:dark cycle. Prior to the start of the
139 experiment, cultured *D. acuminata* cells were observed to fluoresce under green light excitation
140 (546 nm) using an inverted optical microscope (Axiovert 135, Zeiss, Germany) equipped with an
141 epifluorescence module.

142 Optimal gain and threshold settings were identified for the two separate photomultiplier
143 tubes (PMTs), one for side scattering and the other for fluorescence, that are used to trigger IFCB
144 image acquisition. The gain (called PMT A for side scattering and PMT B for fluorescence) is

145 used to adjust the sensitivity of the PMT while the threshold (called trig A for side scattering and
146 trig B for fluorescence) determines the minimum value that the side scattering or fluorescence
147 signal needs to reach in order to trigger imaging of the particle by the camera. Higher gains and
148 lower thresholds will increase sensitivity for detecting and capturing images of smaller particles
149 (when side scattering triggers image acquisition) or particles containing less chlorophyll (when
150 fluorescence triggers image acquisition), but at the cost of higher noise. Higher gain settings can
151 also reduce dynamic range as large particles may saturate the PMT signal. High detection
152 sensitivity (i.e., higher gains and lower thresholds), combined with a high abundance of particles,
153 can reduce the effective volume analyzed per sample due to high inhibit time. Inhibit time is the
154 amount of time that the IFCB is unable to image new particles in the flow cell because it is busy
155 imaging the previously detected particle (IFCB image acquisition is limited to ~14 images per
156 second). Samples with high inhibit time can lead to very low total volumes analyzed per sample
157 resulting in less accurate estimates of target species abundances. Adjusting the gain and
158 threshold settings is therefore a balance of offering sufficient sensitivity to detect target species
159 while limiting the detection of non-target/uninteresting particles and avoiding saturation of the
160 PMT signal.

161 A series of IFCB measurements were made on the same *D. acuminata* (DANY1) culture.
162 Due to the wide-range of possible PMT setting combinations on the IFCB, a preliminary study
163 was performed on the *D. acuminata* culture to select the most appropriate range of PMT gain and
164 threshold settings to quantitatively evaluate performance during the experiment. As a first pass,
165 the threshold was set to a low value (0.125 V) and a broad range of PMT gains were iteratively
166 tested by changing the PMT gain with a coarse resolution (0.1 V increasing steps), while the
167 IFCB was analyzing the culture. It was observed that *D. acuminata* cells were poorly or not

168 detected with gain values lower than 0.3 for PMT A and 0.6 for PMT B. These preliminary
169 results were used to select the range over which the detection of *D. acuminata* was quantitatively
170 evaluated. For each PMT channel (PMT A and PMT B), a total of 12 settings were quantitatively
171 evaluated, each corresponding to a gain and threshold combination. Four PMT B gains (0.60,
172 0.70, 0.80, and 0.90 V) were combined with three threshold (trig B) settings (0.125, 0.140, and
173 0.160 V), and four PMT A gains (0.30, 0.40, 0.50, and 0.60 V) were combined with three
174 threshold (trig A) settings (0.16, 0.20, and 0.25 V). To avoid any potential interaction of the two
175 channels, PMT A and trig A were both set to zero volts when measurements were made using the
176 PMT B channel and vice versa. For each combination of gain and threshold settings, the IFCB
177 was set to analyze 1 mL. Before each sample, the sample tube was flushed and the intake line
178 was primed with 1 mL of the sample to prevent carryover from the prior sample. For each
179 combination of settings, the IFCB measurements were made in triplicate by measuring three
180 separate 1 mL samples. All measurements were made within 2 days (one day for all
181 measurements with side scattering and a second day for all measurements with fluorescence) to
182 ensure that the *Dinophysis* spp. culture remained consistent across samples. The cellular
183 biovolume of *D. acuminata* is lower than other species of *Dinophysis* found in Puget Sound, and
184 strains of *D. acuminata* isolated from the Northeast/Mid-Atlantic coast (including DANY1) have
185 a lower biovolume compared to strains from the Pacific Northwest (Ayache et al. 2023).
186 Therefore, the optimal IFCB settings identified during the experiments are conservative and
187 likely more sensitive than what is required to detect the suite of *Dinophysis* species in Puget
188 Sound. The abundance of *D. acuminata* DANY1 in the culture was also determined
189 microscopically on each day of the IFCB measurements. A sample of the culture was fixed with
190 70% ethanol and all of the *Dinophysis* spp. cells were counted in 1 mL sub-samples by observing

191 the gridded Sedgwick Rafter chamber in its totality under an inverted optical microscope
192 (Axiovert 135, Zeiss, Germany) at 100 x magnification.

193

194 2.2. *In situ Dinophysis spp. observations*

195 2.2.1. *Study site*

196

197 This study leveraged an existing time series of IFCB observations in Puget Sound
198 collected as part of a larger cross-regional comparison of *Dinophysis spp.* bloom dynamics in the
199 U.S. The study site is located at the terminal end of Budd Inlet in southern Puget Sound,
200 Washington State (Fig. 1). This area is both a hotspot for *Dinophysis spp.* blooms (Trainer and
201 King 2023; Trainer et al. 2013) and a top shellfish producing region contributing up to 37% of
202 total production and almost 58% of the \$270 million total value in Washington State
203 (Washington Sea Grant 2015). Washington's highest recorded value of DST (250 μg DST / 100
204 g of shellfish) was measured in blue mussels from Budd Inlet in 2016 (PSEMP Marine Waters
205 Workgroup 2017) - a value well above the federal standard for human consumption of 16 μg /
206 100 g of shellfish (FDA 2011).

207 Budd Inlet, located near the city of Olympia, is a narrow, elongated inlet that stretches
208 approximately 2.5 km wide by 11 kilometers long. The inlet is shallow with less than 11 m depth
209 in the south and 27 m depth in the north. Tides are semidiurnal with an average range of 4.4 m.
210 The southern part of Budd Inlet receives freshwater from the Deschutes River which flows
211 through the Capitol Lake dam while the northern part receives seawater from South Puget
212 Sound. The tide tends to create counter-clockwise flow patterns and sometimes a gyre forms in
213 the center of Budd Inlet (Boatman et al. 2000).

214 2.2.2. Puget Sound IFCB deployment

215

216 The IFCB was deployed from a floating boathouse at the Olympia Yacht Club from
217 March 31 to September 27, 2022. The IFCB intake was located at 1.7 m depth and was
218 terminated with a 1-mm copper pre-filter followed by a 150- μ m Nitex mesh to prevent
219 biofouling and large particles from clogging the internal fluidics system. The IFCB was
220 configured to continuously analyze 5 mL samples and to alternate between side scattering and
221 fluorescence-based image acquisition. Fluorescence (PMT B = 0.60 V and trig B = 0.125 V) was
222 primarily used to trigger image acquisition, with samples analyzed using side scattering (PMT A
223 = 0.50 V and trig A = 0.250 V) to trigger image acquisition interspersed throughout the
224 deployment approximately twice a day (every 30 samples). The IFCB observations were served
225 on an IFCB dashboard hosted by the Harmful Algal Bloom Observing Network ([https://habon-](https://habon-
226 ifcb.whoi.edu/buddinlet)

227 A classifier that automates taxonomic classification of images was not used in this study.
228 Instead, for each day of the deployment, one side scatter sample and the fluorescence sample
229 immediately preceding or following it (206 samples total) were visually inspected and manually
230 identified using publicly available MATLAB-based annotation tools
231 (<https://github.com/hsosik/ifcb-analysis>). *Dinophysis* spp. cells were manually classified to the
232 species level when possible or to genus level if their orientation did not provide a view of
233 distinguishing criteria required for their identification (e.g., when they were pictured in apical or
234 antapical views or when their left sulcal list was not clearly visible). This enabled the accurate
235 counting and identification of the different *Dinophysis* species in the samples; something which
236 can sometimes be difficult to reach with a classifier.

237 Measures of the level of autofluorescence of each phytoplankton cell that was sampled by
238 the IFCB (IFCB-autofluorescence) were extracted from the adc files (PMT B column). Of note,
239 these measures are available for each cell regardless of the method used to trigger image
240 acquisition such that IFCB-autofluorescence measures were also obtained when the triggering
241 method was side scattering (and vice versa).

242 Biovolume of each phytoplankton cell was extracted from the features files by following
243 the blob and features extraction procedure (v2) available on github
244 (<https://github.com/hsosik/ifcb-analysis>). This procedure implements the Moberg and Sosik
245 (2012) algorithm that uses distance maps to estimate cell volume from two-dimensional plankton
246 images. Biovolume was converted from pixels to μm^3 using an estimated conversion factor of
247 3.81 pixels/micron determined from more than 1,000 IFCB images of 5.7 μm fluorescent beads
248 collected on different dates during the deployment.

249 To compare the IFCB measurements to conventional microscopy, discrete water samples
250 were manually collected approximately weekly for observations of *Dinophysis* spp. cells,
251 resulting in 18 samples total. A 2-L Niskin bottle was used to collect water samples at 1.5 m
252 depth, which was slightly shallower than the placement of the IFCB intake. This sampling depth
253 was chosen because it was where the highest chlorophyll concentrations were most often
254 observed during preliminary sampling. Immediately upon returning to the laboratory, the discrete
255 water sample was fixed with 70% ethanol and *Dinophysis* spp. cells were enumerated at 100 x
256 magnification using an inverted optical microscope (Axiovert 135, Zeiss, Germany) equipped
257 with an epifluorescence module. To enable better comparison with the IFCB and match the 5 mL
258 that the IFCB was configured to sample, all of the *Dinophysis* spp. cells were enumerated
259 microscopically in a 5 mL sample without concentrating the sample and without replication. Five

260 1 mL sub-samples were transferred to a gridded Sedgwick Rafter chamber and each *Dinophysis*
261 species was counted under the microscope and summed across sub-samples. The proportion of
262 *Dinophysis* spp. cells exhibiting autofluorescence was also determine by microscopy under green
263 light excitation with a fluorescence cube equipped with a green H 546 filter (excitation 546 nm).

264

265 2.3 Statistical analyses

266 2.3.1. Optimization of IFCB settings

267

268 Two-way ANOVAs followed by post-hoc pairwise multiple comparisons using the
269 Holm-Šidák method (Holm 1979) were employed to assess the effects of the different gain and
270 threshold settings, and their interactions, on the effective sample volume analyzed by the IFCB
271 and IFCB estimates of *D. acuminata* abundances and total number of particles. Separate two-
272 way ANOVAs were conducted for the side scattering (PMT A) and fluorescence-based (PMT B)
273 triggering methods. Separate one-way ANOVAs (for PMT A and PMT B) followed by post-hoc
274 multiple comparisons versus a control group with the Holm-Šidák method (Holm 1979) were
275 used to test for differences between *D. acuminata* cell abundances determined by microscopy
276 and the IFCB measurements made using the 12 PMT gain and threshold setting combinations.
277 Before ANOVA analyses, normality and equal variance were tested using the Shapiro-Wilk
278 (Royston 1982) and Brown-Forsythe (Brown and Forsythe 1974) tests, respectively. All analyses
279 were performed using SigmaPlot 14.0.

280

281

282 2.3.2. *In situ Dinophysis spp. observations*

283

284 The significance of differences in the total abundance of *Dinophysis* spp. cells detected *in*
285 *situ* by the IFCB using side scattering and fluorescence-based triggering methods were tested
286 with a Mann-Whitney U test. A second Mann-Whitney U test was used to test for significant
287 differences in the total abundance of *Dinophysis* cells detected by the IFCB and determined from
288 microscope counts. A permutational multivariate analysis of variance (PERMANOVA,
289 Anderson 2017) was used to test for significant difference in *Dinophysis* species composition
290 determined using the side scattering and fluorescence-based triggering methods. PERMANOVA
291 is a resemblance-based permutational method allowing to perform variance partitioning based on
292 F statistics, like ANOVA, for testing the simultaneous response of several variables to one or
293 several factors with the advantage of not requiring data normality. *Dinophysis* species
294 abundances were fourth root transformed before the PERMANOVA analysis to down-weight the
295 importance of the highly abundant species and to take into account the rarer species in the
296 calculation of the similarity matrix. The PERMANOVA analysis was based on a Bray-Curtis
297 similarity matrix and 9999 permutations were run. The PERMANOVA analysis was performed
298 with the function “adonis” available in the R vegan package (Oksanen et al. 2018). A linear
299 regression model was used to study the relationship between the IFCB-autofluorescence level
300 and biovolume of *Dinophysis* species cells with the function “lm” available in the R stats
301 package. Spearman’s correlation was used to evaluate the relationship between the biovolume
302 and IFCB-autofluorescence of *Mesodinium* spp. cells using the function “cor.test” available in
303 the R stats package.

304

305 3. Results

306 3.1. Optimization of IFCB settings

307

308 Different PMT gain and threshold setting combinations significantly affected the
309 detection of *D. acuminata* cells in culture by the IFCB using either side scattering or
310 fluorescence-based triggering methods. For both methods, *D. acuminata* abundance estimates
311 were significantly different for the tested setting combinations and there was a significant
312 interaction between the PMT gain and threshold (two-way ANOVA $p < 0.01$ Tables S1 and S2,
313 Fig. 2).

314 For side scattering image acquisition, PMT A gain settings of 0.30 and 0.40 V
315 underestimated *D. acuminata* abundance for all of the threshold (trig A) settings evaluated (one-
316 way ANOVA, $p < 0.05$ Table S3, Fig. 2 A). A PMT A gain setting of 0.30 V only detected 6-26%
317 of the *D. acuminata* abundance determined microscopically, and a PMT A gain setting of 0.40 V
318 detected 54-80% of *D. acuminata* abundance. PMT A gain settings of 0.50 and 0.60 V provided
319 *D. acuminata* abundance estimates not significantly different from the microscopic counts for all
320 of the trig A settings evaluated except with the combination of PMT A gain = 0.60 V and trig A
321 = 0.25 V which resulted in a higher abundance (Table S3, Fig. 2 A). The PMT gain and threshold
322 settings also influenced the effective volume analyzed and total number of particles detected by
323 the IFCB with a significant interaction between the PMT A gain voltage and trig A voltage (two-
324 way ANOVA $p < 0.001$ Tables S4 and S5, Fig. 2 C&E). Increasing the PMT A gain voltage
325 resulted in a lower effective volume analyzed and higher number of (non-target/uninteresting)
326 particles detected. For a given PMT A gain voltage, the effective volume analyzed was
327 proportional to the trig A voltage, while the total number of particles detected was inversely

328 proportional to the trig A voltage. Some trig A combinations with the PMT A gain = 0.50 and
329 0.60 V settings were so sensitive to small particles in the *D. acuminata* culture that the effective
330 volume analyzed was only 0.51-0.68 mL instead of the 1 mL that the IFCB was programmed to
331 sample.

332 For fluorescence-based image acquisition, *D. acuminata* abundance was underestimated
333 in comparison to the microscopic counts for all PMT gain and threshold setting combinations
334 except for the combination of PMT B gain = 0.80 V and threshold trig B = 0.125 V (Fig. 2 B,
335 one-way ANOVA $p < 0.05$ Table S6). The PMT B gain settings of 0.60 and 0.70 V provided the
336 lowest abundance estimates, only detecting 1-51% and 26-87% of *D. acuminata* cells
337 respectively. *D. acuminata* abundance estimates obtained with the PMT B gain settings = 0.80 V
338 and 0.90 V were not significantly different from each other and were closest to the microscopic
339 counts. However, when these gain settings were combined with the lowest thresholds (trig B =
340 0.140 and 0.125 V), sometimes the acquisition of images was triggered but no particle was
341 detected on the images. IFCB users call this phenomenon “triggers with zero region of interest
342 (ROI)”. This can occur for high gain combined with low threshold due to electrical noise that can
343 sometimes be sufficient to trigger image acquisition when there is no real particle. It can also
344 occur for certain combinations of other settings within the IFCB configuration (i.e.,
345 blobXgrowAmount, blobYgrowAmount, and minimumBlobArea) when high gain is combined
346 with low threshold settings and tiny debris is detected - in this case, the trigger is real but the
347 ROI is too small to be saved based on the configuration settings. The combination of PMT B
348 gain = 0.90 V and trig B = 0.140 V saturated the IFCB with triggers with zero ROI (98% of
349 triggers with zero ROI Fig. 2H) and the effective volume analyzed was only 0.1 mL of the 1 mL
350 sample (Fig. 2 D). The same phenomenon occurred with the combination PMT B gain = 0.80

351 and trig B = 0.125 which only analyzed 0.16-0.36 mL of the 1 mL sample and resulted in 95% of
352 triggers with zero ROI. With the combination of PMT B = 0.90 V and trig B = 0.125, the number
353 of triggers with zero ROI was so high that the IFCB was unable to manage them and the software
354 IFCBacquire stopped running before the sample could be completely analyzed. In contrast to
355 PMT B, none of the settings tested for PMT A resulted in a high proportion of triggers with zero
356 ROI (Fig. 2 G).

357 Similarly to the PMT A experiment, the PMT B gain and threshold settings influenced
358 the effective volume analyzed and total number of particles detected by the IFCB with a
359 significant interaction between the PMT B gain voltage and trig B voltage (two-way ANOVA
360 $p < 0.001$ Tables S7 and S8, Fig. 2 D&F). Increasing the PMT B voltage resulted in a higher
361 number of particles detected and for a given PMT B voltage, the total number of particles
362 detected was inversely proportional to the trig B voltage; however, contrary to the PMT A
363 experiment, the majority of particles detected were *D. acuminata* cells with just a small number
364 of non target/uninteresting particles (Fig. 2 F).

365 Optimal settings were identified as those that provided abundances not significantly
366 different from the microscopic counts, analyzed the near-total sample volume, and minimized the
367 detection of small debris. The combination of PMT A = 0.50 V with trig A = 0.20 or 0.25 V was
368 identified as the best setting to detect *D. acuminata* in culture using the side scattering. The best
369 settings to detect *D. acuminata* using the fluorescence triggering were determined to be PMT B =
370 0.80 V and trig B = 0.140 V.

371 The optimal gain and threshold settings identified here for *D. acuminata* in culture
372 correspond to the settings that were used to acquire the existing time series of IFCB observations
373 in Budd Inlet for the side scattering triggering method (PMT A = 0.50 V and trig A = 0.25 V),

374 but not for fluorescence. The gain setting used for fluorescence-based image acquisition in the
375 field was less sensitive than the setting found to be optimal in the laboratory experiments, but the
376 threshold setting was lower (PMT B = 0.60 V and trig B = 0.125 V in the field vs. PMT B = 0.80
377 V and trig B = 0.140 V in the laboratory for *D. acuminata* in culture).

378

379 3.2 *In situ* *Dinophysis* spp. observations

380 3.2.1. *Dinophysis* spp. and *Mesodinium* spp. bloom dynamics

381

382 Two blooms of *Dinophysis* spp. were observed by microscopy and the IFCB in Budd
383 Inlet from March 31 to September 27, 2022. The first bloom occurred from June to mid-July
384 (“June-July bloom” hereafter) and was primarily composed of *Dinophysis fortii*, *D. acuminata*,
385 and *Dinophysis norvegica*. The maximum density of *Dinophysis* spp. detected by the IFCB
386 during the June-July bloom was 4,682 cells L⁻¹ on June 30th. Weekly microscopy sampling
387 detected 8,000 cells L⁻¹ two weeks later on July 14th, but IFCB data were not available at that
388 time due to instrument maintenance. The June-July *Dinophysis* spp. bloom was preceded by a
389 bloom of *Mesodinium* spp. that started at the end of May and lasted until the end of June (Fig. 3
390 A&B). The second *Dinophysis* spp. bloom occurred at the end of September (“September
391 bloom” hereafter) and was dominated by *D. fortii* (Fig. 3 A&B). The maximum density of
392 *Dinophysis* spp. detected by the IFCB was 6,657 cells L⁻¹ on September 22nd. The September
393 bloom coincided with a second bloom of *Mesodinium* spp. Two other *Dinophysis* species were
394 observed during the deployment. *Dinophysis parva* was detected at low abundances in July,
395 August, and early September. *Dinophysis odiosa* was detected at low abundances on only two

396 occasions: September 19th and 27th. A small number of dividing and fusing *Dinophysis* spp. cells
397 were detected at the beginning of the June-July bloom and at the end of August (data not shown).

398

399 *3.2.2. Side scattering versus fluorescence-based detection of Dinophysis spp. in*
400 *relation to Mesodinium spp. abundance*

401

402 The temporal dynamics of *Dinophysis* spp. abundance determined by the IFCB using side
403 scattering and fluorescence-based triggering methods were similar to one another and were
404 similar to patterns determined from the microscopic counts (Fig. 3 A&B); however, in
405 comparison to microscopic counts, the IFCB underestimated the total abundance of *Dinophysis*
406 spp. regardless of the method used to trigger image acquisition (Mann-Whitney U test, $p < 0.05$).
407 Even though the field settings for fluorescence-based image acquisition were found to be less
408 sensitive than the optimal settings identified in the laboratory for *D. acuminata* in culture, there
409 were no significant differences in *Dinophysis* species composition determined using the two
410 triggering methods; that is, both methods performed equally in the detection of all five species of
411 *Dinophysis* observed (PERMANOVA, $p > 0.05$, Fig. 3 A&B). However, in some samples, the
412 side scattering triggering method detected more *Mesodinium* spp. cells than the fluorescence
413 triggering method. For example, approximately two times more *Mesodinium* spp. cells were
414 detected using side scattering compared to fluorescence triggering method in June (maximum
415 abundance of 5,609 *Mesodinium* spp. cells L⁻¹ detected with the side scattering vs. 2,460 cells L⁻¹
416 detected by triggering on fluorescence) and September (maximum abundance of 10,636
417 *Mesodinium* spp. cells L⁻¹ detected with the side scattering vs. 4,422 cells L⁻¹ detected by
418 triggering on fluorescence).

419 Towards the end of the June-July bloom, there was also a 7-day period when there was a
420 significant difference in the total abundance of *Dinophysis* spp. cells detected using the two
421 triggering methods (Mann-Whitney U test, $p < 0.05$). During this period (highlighted in gray on
422 Fig. 3 A&B), the side scattering triggering method detected low abundances of *Dinophysis* spp.
423 cells (the presence of which was confirmed by microscopy) while the fluorescence triggering
424 method did not detect any cells. The proportion of fluorescent *Dinophysis* spp. cells observed by
425 microscopy during this period was the lowest observed during the entire deployment and the
426 level of autofluorescence of *Dinophysis* spp. cells measured by the IFCB decreased (Fig. 3 C).
427 The size and level of IFCB-autofluorescence of *Dinophysis* spp. cells were significantly and
428 positively correlated (Fig. 4), but this correlation only explained 28% of the variability and did
429 not explain the difference in detection of *Dinophysis* spp. cells between the two triggering
430 methods observed during this 7-day period. Indeed, while there were some samples with
431 *Dinophysis* spp. cells presenting a low biovolume ($< 20,000 \mu\text{m}^3$) during this period, there were
432 also samples with cells presenting a high biovolume (31,513 to 37,718 μm^3). Further, at other
433 times during the deployment, some *D. fortii* with similar size presented very different levels of
434 IFCB-autofluorescence. This suggests that the physiological status of the *Dinophysis* spp. cells
435 may have contributed to variability in their autofluorescence which resulted in the inability of the
436 IFCB to detect them when triggering on fluorescence.

437 The level of IFCB-autofluorescence of *Dinophysis* spp. cells and proportion of
438 *Dinophysis* spp. cells exhibiting fluorescence observed by microscopy (Fig. 3 C) covaried with
439 the abundance of *Mesodinium* spp. (Fig. 3 A & B). In June, when *Dinophysis* spp. co-occurred
440 with *Mesodinium* spp., the level of IFCB-autofluorescence of *Dinophysis* spp. cells ranged from
441 0.007 to 0.094. After the disappearance of *Mesodinium* spp. in July, the level of IFCB-

442 autofluorescence of *Dinophysis* spp. cells progressively decreased and reached a minimum
443 average value of 0.015. IFCB-autofluorescence levels of *Dinophysis* spp. cells remained
444 relatively low until September when they reached the highest levels observed during the
445 deployment, coinciding with the second bloom of *Mesodinium* spp. and the September bloom of
446 *Dinophysis* spp.

447 A wide range of *Mesodinium* spp. cell sizes were observed during the deployment, with
448 biovolume ranging from 28 to 59,051 μm^3 (Fig. 5 A). The first bloom of *Mesodinium* spp.
449 presented a wider range in cell size than the second bloom, but the majority of *Mesodinium* spp.
450 cells measured 28 to 10,000 μm^3 . In contrast, during the second bloom, the majority of
451 *Mesodinium* spp. cells presented a bigger size (5,000 to 15,000 μm^3). The biovolume and level of
452 IFCB-autofluorescence of *Mesodinium* spp. cells were positively correlated ($r = 0.71$, $p < 0.001$)
453 (Fig. 5 B).

454

455 **4. Discussion**

456

457 The IFCB failed to detect *Dinophysis* spp. *in situ* using the fluorescence triggering
458 method when the IFCB-autofluorescence level of individual cells was low and when the
459 proportion of cells exhibiting autofluorescence determined by microscopy was less than 50%.
460 This was observed during a 7-day period towards the end of the June-July bloom, when cells
461 were still detected using the side scattering triggering method. It is worth noting that the IFCB
462 gain and threshold settings used in the field were less sensitive than the optimal settings for
463 fluorescence-based image acquisition of *Dinophysis acuminata* determined from the laboratory
464 experiments. In the case of *Dinophysis* spp. and likely other mixotrophic dinoflagellates, PMT B

465 settings for fluorescence-based image acquisition need to be fairly sensitive to detect starved
466 cells and/or the side scattering triggering method may need to be used to ensure their detection.
467 Given the growing interest in using IFCBs to monitor HABs and initiate management actions,
468 robust IFCB calibration procedures, such as the approach used in this study, are critical to ensure
469 accurate detection of HAB species.

470 The results of this study highlight the importance of intentionally selecting the triggering
471 method (side scattering and/or fluorescence) for image acquisition by the IFCB, as well as
472 quantitatively tuning the gain and threshold settings. Fluorescence-based image acquisition is
473 commonly used for HAB (and phytoplankton) monitoring and detection in nearshore
474 environments to avoid interference by high abundances of detritus; however, this method may
475 not always be suitable for detecting *Dinophysis* spp. and other non-constitutive mixotrophic
476 species like *Mesodinium* spp. or green *Noctiluca scintillans*. The autofluorescence of these
477 species depends on prey availability or physiological status of symbionts. As such, fluorescence-
478 based image acquisition can undercount or entirely miss starved cells exhibiting low or no
479 autofluorescence. In contrast, the side scattering triggering method detects all particles that
480 scatter light and will consequently image non-fluorescing cells that may be missed by the
481 fluorescence-based triggering method. Side scattering may also provide a better understanding of
482 biotic interactions because it will image target HAB species as well as the surrounding
483 community, inclusive of non-fluorescing heterotrophic dinoflagellates and small zooplankton.
484 For example, *in situ* IFCB samples analyzed using the side scattering triggering method in this
485 study detected significantly more *Mesodinium* spp. compared to the fluorescence triggering
486 method, providing insight into predator-prey dynamics. In environments that have high

487 abundances of detritus with a size range close to target HAB species, however, the side
488 scattering triggering method can introduce error due to the inhibit time.

489 As expected, in this study, inhibit times for *in situ* samples analyzed using the side
490 scattering triggering method were consistently higher than for the fluorescence triggering method
491 with the exception of two samples over the entire deployment duration (data not shown). As a
492 result, the effective volume analyzed by side scattering was on average 0.57 mL less than that
493 analyzed by fluorescence (note that the IFCB was configured to sample 5 mL). These results are
494 representative of an inherent trade-off in selecting a triggering method whereby the fluorescence
495 triggering method typically has lower inhibit times due to reduced interference from detritus but
496 can miss particles with lower autofluorescence. Approaches that IFCB users can consider to
497 balance this trade-off and more accurately detect non-constitutive mixotrophic species like
498 *Dinophysis* spp. during starvation include: 1) alternating triggering between side scattering and
499 fluorescence (as was done in this study), 2) triggering with both side scattering and fluorescence,
500 or 3) increasing the sensitivity of PMT B and pooling samples. Alternating between both
501 triggering methods allow users to take advantage of the lower inhibit times from the fluorescence
502 method, while using the side scattering method to ensure that they are not missing cells
503 exhibiting low or no autofluorescence. For the second option, both PMT channels (PMT A and
504 PMT B) are tuned on and the IFCB triggers with an “OR” logic such that a particle exhibiting
505 low fluorescence (e.g., a starved *Dinophysis* spp. cell) that does not meet the threshold for
506 triggering on PMT B may still trigger on PMT A. In this scenario, careful tuning would be
507 needed to decrease the side scattering sensitivity to filter out small particles and detritus to avoid
508 introducing error due to high inhibit times and to increase the fluorescence sensitivity to more
509 accurately detect prey (i.e., small *Mesodinium* spp.). For the third option, only PMT B would be

510 turned on for sampling but with the fluorescence sensitivity increased to detect weakly
511 fluorescing *Dinophysis* spp. cells. To offset the potential reduced sample volume due to higher
512 inhibit time – a trade-off of increasing sensitivity – multiple samples (i.e., IFCB syringe pulls)
513 could be pooled to get more accurate estimates of species abundances. Of note, a modified
514 version of the IFCB has been developed that carries out automated live cell fluorescent staining
515 to improve the detection of organisms that don't exhibit autofluorescence (IFCB-S; Brownlee et
516 al. 2016). While there are no plans to commercialize the IFCB-S at this time, it represents an
517 important step in the evolution of new strategies for automated detection of starved mixotrophs,
518 like *Dinophysis* spp., or herbivorous microzooplankton.

519 Once the IFCB triggering method has been chosen, the gain and threshold settings need
520 to be tuned. Two commonly used approaches for tuning the gain and threshold settings of the
521 IFCB are to: 1) image as wide a size range of phytoplankton as possible, or 2) optimize the
522 detection of target species. The best approach will differ depending on the application. For
523 example, tuning the IFCB using the first approach would be most suited if the goal is to study
524 HAB dynamics in relation to the surrounding phytoplankton community. Alternatively, the
525 second tuning approach would be most appropriate if the goal is to accurately quantify a target
526 species and provide early warning of HAB events based on abundance thresholds. Fine tuning
527 the PMT settings using this approach screens out particles that are not of interest and increases
528 the likelihood of detecting target HAB species even when they are present at low abundances. In
529 the case of *Dinophysis* spp., if the goal is to study how the predator/prey relationships influence
530 *Dinophysis* spp. ecology, the PMT settings will need to be adjusted to accurately detect both
531 *Mesodinium* spp. and *Dinophysis* spp.

532 This study introduces an approach for tuning an IFCB to optimize detection of a target
533 species and demonstrates the effects of a poorly-calibrated IFCB. The most optimal settings were
534 found by iteratively adjusting the PMT gain and threshold settings so that the number of *D.*
535 *acuminata* cells imaged by the IFCB was as close as possible to the microscope count from the
536 same sample. The laboratory experiments showed that non-optimal settings missed a significant
537 proportion of *D. acuminata* abundance whatever the method used to trigger the images
538 acquisition. *Dinophysis* spp. can present acute toxicity at low abundances (e.g., Yasumoto et al.
539 1985), so a poorly-calibrated IFCB may not provide HAB early warning. The optimal PMTs gain
540 and threshold settings identified in this study may provide a good starting point for other IFCB
541 users wishing to tune their IFCB to target *Dinophysis* spp. However, due to inherent differences
542 across instruments which make each IFCB a unique instrument, IFCB detection settings are not
543 directly transferable and the users will still need to reproduce the calibration approach presented
544 here with their own instrument. For example, two IFCBs with the same PMT settings deployed
545 in tandem in the Monterey Bay produced different phytoplankton cell concentrations
546 (McGaraghan et al. 2022). Although a single strain culture was used to demonstrate the
547 calibration approach, IFCB settings may also need to be further refined for *in situ* sampling.
548 Natural samples not only have different strains of the target species with variable
549 autofluorescence, but also a diversity of other phytoplankton. For example, when the optimal
550 settings for fluorescence identified in the laboratory study were applied to a discrete, natural
551 sample from Budd Inlet spiked with a known number of cultured *D. acuminata* cells, high
552 abundances of nanoplankton were sampled and the PMT B settings needed to be adjusted down
553 to accurately quantify *D. acuminata* (data not shown). Therefore, while optimal IFCB settings

554 determined using cultures provide an ideal starting place, further tuning with natural samples
555 may still be required.

556 The field results of this study demonstrated that the physiological status of *Dinophysis*
557 spp. can influence detection by the IFCB. Overall, both IFCB triggering methods provided a
558 similar view of *Dinophysis* spp. temporal dynamics, except during a 7-day period towards the
559 end of the June-July bloom when fluorescence did not trigger *Dinophysis* spp. cells, but side
560 scattering did. The June-July bloom of *Dinophysis* spp. was preceded by a bloom of *Mesodinium*
561 spp., which started to decline from mid-June until *Mesodinium* spp. was no longer detected in
562 July. After this period, the proportion of fluorescing *Dinophysis* spp. cells determined by
563 microscopy and autofluorescence of individual cells measured with the IFCB progressively
564 decreased, and reached their lowest point when the IFCB fluorescence triggering method did not
565 detect any *Dinophysis* spp. cells, but the scattering triggering method did. Together, this suggests
566 that starved *Dinophysis* spp. cells were not adequately detected by the IFCB.

567 The decrease in autofluorescence of *Dinophysis* spp. cells observed by microscopy and
568 by the IFCB about one month after the decline of the *Mesodinium* spp. bloom is in line with
569 findings from laboratory experiments showing the effect of starvation on *D. fortii* and *D. caudata*
570 (Nagai et al. 2008; Park et al. 2008). These studies showed that in absence of prey, the plastids
571 that *D. fortii* and *D. caudata* previously sequestered remained functional for 1-2 months but the
572 autofluorescence of the cells and their photosynthetic ability decreased during the starvation. Of
573 note, starved *D. caudata* cells can reacquire plastids and recover their autofluorescence as soon
574 as one day after addition of *Mesodinium rubrum* in the laboratory cultures (Park et al. 2008). In a
575 field setting, this rapid recovery of autofluorescence, and hence detection by the IFCB using
576 fluorescence triggering, could complicate efforts to determine the source of *Dinophysis* spp. cells

577 and understand bloom initiation and predator-prey dynamics (e.g., whether *Dinophysis* spp. cells
578 were advected into a region or a local population of starved cells were exposed to prey).

579 The highest values of IFCB-autofluorescence of *Dinophysis* spp. cells were observed
580 during the September bloom. In contrast to the June-July bloom of *Dinophysis* spp., which
581 lagged peak abundances of *Mesodinium* spp., the September bloom of *Dinophysis* spp. co-
582 occurred with a bloom of large *Mesodinium* spp. The presence of *Mesodinium* spp. throughout
583 the September bloom would have provided a sustained source of plastids that *Dinophysis* spp.
584 could acquire, thus increasing autofluorescence. Additionally, the biovolume of *Mesodinium* spp.
585 cells were found to be positively correlated with their IFCB-autofluorescence, demonstrating that
586 larger cells of *Mesodinium* spp. have more plastids. The larger and more nutritious cells of
587 *Mesodinium* spp. during the September bloom provide another reason for the high levels of
588 *Dinophysis* spp. IFCB-autofluorescence. This finding is supported by laboratory (Smith et al.
589 2018) and field studies (Harred and Campbell 2014), which have observed that larger
590 *Mesodinium* spp. cells are more nutritious and support faster growth rates and higher biomass of
591 *Dinophysis* spp. However, the potential for other environmental factors, such as light intensity
592 (Nielsen et al. 2012) and nutrient availability (Parkhill et al. 2001), to influence the
593 autofluorescence of *Dinophysis* spp. cells cannot be ruled out. A controlled laboratory
594 experiment would be needed to explore the effect of starvation on detection of *Dinophysis* spp.
595 cells by the IFCB in the absence of other variables.

596 To avoid acute health risks, it is essential that IFCB monitoring programs can accurately
597 detect both starved cells with reduced autofluorescence and low cell abundances, because starved
598 cells can still contain toxins. Laboratory experiments have found higher cellular toxin quotas for
599 DSTs (i.e., okadaic acid, dinophysistoxin-1b, dinophysistoxin-2 and pectenotoxin-2) in prey-

600 depleted, senescent cultures compared to well-fed, exponentially growing cultures (García-
601 Portela et al. 2018; Nielsen et al. 2012; Nielsen et al. 2013). This occurs because toxin
602 production continues while growth rates decline, resulting in an accumulation of toxins in cells.
603 Evidence of this has also been found in the field (e.g., Pizarro et al. 2008). It is the product of
604 *Dinophysis* spp. cell abundance and cell toxicity that influences shellfish toxicity and the
605 resulting risk for DSP (García-Altarets et al. 2016; Reguera et al. 2014) but high abundances are
606 not a requirement for *Dinophysis* spp. cells representing a risk. For instance, Lindahl et al. (2007)
607 indicated that approximately 100 highly toxic cells from a low-density population of *D.*
608 *acuminata* may lead to the same accumulation of DSP in a mussel as the ingestion of 1,500 low
609 toxic cells from a higher density population. Further, because *Dinophysis* spp. can reacquire
610 plastids after a period of starvation (Park et al. 2008), in the field, such populations of highly-
611 toxic prey-limited *Dinophysis* spp. could become a “seed” population able to recover and
612 potentially bloom after the return of *Mesodinium* spp.

613

614 5. *Conclusion*

615

616 The IFCB is increasingly being used to rapidly and autonomously detect developing
617 HABs *in situ* and provide insight into aspects of HAB ecology. It is therefore important to
618 consider best practices and develop standardized approaches to ensure accurate detection of
619 HAB species and facilitate comparison of IFCB data products across instruments and user
620 groups. This study demonstrates a quantitative approach to tune the IFCB settings to optimize
621 detection of a target HAB taxon and highlights the trade-offs associated with choosing a
622 triggering method for image acquisition. Fluorescence-based image acquisition in environments

623 with high detritus will lower inhibit times relative to side scattering, but may miss the detection
624 of non-constitutive mixotrophic species like *Dinophysis* spp. when prey is limited. If the target
625 HAB is a mixotrophic species, one path forward is to alternate sampling with the fluorescence
626 and side scattering triggering methods. Having both types of measurements in this study allowed
627 us to determine that the temporary disappearance of *Dinophysis* spp. from the fluorescence
628 triggering record was likely caused by starvation. Given the effect that IFCB settings have on
629 data quality, users should consider reporting both their calibration procedure and IFCB settings
630 to better compare measurements across the IFCB user community.

631

632 **Acknowledgements**

633 We thank Nour Ayache, Megan Ladds, James Fiorendino and Lisa Campbell for
634 providing isolates of *Dinophysis* spp., *Mesodinium rubrum*, and *Teleaulax amphioxeia* and for
635 their precious advice on *Dinophysis* spp. culturing. For their technical assistance with IFCB
636 maintenance, we thank Tom Fougere, Vinnie Ferreira and Ivory Engstrom. We thank Mark
637 Fleischer for providing access to his boathouse and Vera Trainer for support during the IFCB
638 field deployment and assistance in the writing of the Fulbright proposal.

639

640 **Funding**

641 This paper is a result of research funded by the National Oceanic and Atmospheric
642 Administration National Centers for Coastal Ocean Science Competitive Research
643 Program under award NA19NOS4780182 to the Virginia Institute of Marine Science. E.H. was
644 awarded a Fulbright Fellowship funded by the Franco-American Fulbright Commission and
645 French region Hauts-de-France. This is ECOHAB publication number ECO1084.

646 **References**

- 647 Anderson, D.M., Andersen, P., Bricelj, V.M., Cullen, J.J., Rensel, J.E.J., 2001. Monitoring and
 648 Management Strategies for Harmful Algal Blooms in Coastal Waters, APEC #201-MR-01.1,
 649 Asia Pacific Economic Program, Singapore, and Intergovernmental Oceanographic Commission
 650 Technical Series No. 59, Paris.
- 651 Anderson, D.M., Cembella, A.D., Hallegraeff, G.M., 2012. Progress in Understanding Harmful
 652 Algal Blooms: Paradigm Shifts and New Technologies for Research, Monitoring, and
 653 Management. *Annu. Rev. Mar. Sci.* 4(1), 143-176.
- 654 Anderson, D.M., Fensin, E., Gobler, C.J., Hoeglund, A.E., Hubbard, K.A., Kulis, D.M.,
 655 Landsberg, J.H., Lefebvre, K.A., Provoost, P., Richlen, M.L., Smith, J.L., Solow, A.R., Trainer,
 656 V.L., 2021. Marine harmful algal blooms (HABs) in the United States: History, current status
 657 and future trends. *Harmful Algae* 102, 101975.
- 658 Anderson, M.J., 2017. Permutational Multivariate Analysis of Variance (PERMANOVA). Wiley
 659 StatsRef: Statistics Reference Online, 1-15.
- 660 Ayache, N., Bill, B.D., Brosnahan, M.L., Campbell, L., Deeds, J.R., Fiorendino, J.M., Gobler,
 661 C.J., Handy, S.M., Harrington, N., Kulis, D.M., McCarron, P., Miles, C.O., Moore, S.K., Nagai,
 662 S., Trainer, V.L., Wolny, J.L., Young, C.S., Smith, J.L., 2023. A survey of *Dinophysis* spp. and
 663 their potential to cause diarrhetic shellfish poisoning in coastal waters of the United States. *J.*
 664 *Phycol.* 00, 1-23.
- 665 Belin, C., Soudant, D., Amzil, Z., 2021. Three decades of data on phytoplankton and
 666 phycotoxins on the French coast: Lessons from REPHY and REPHYTOX. *Harmful Algae* 102,
 667 101733.
- 668 Boatman, C., Cox, J.M., Devol, A., Ebbesmeyer, C.C., Edinger, J., Newton, J., Norton, D., 2000.
 669 Budd Inlet Scientific Study: An overview of findings, LOTT Wastewater Resource Management
 670 Plan, p. 8.
- 671 Brown, C.W., Green, D., Hickey, B.M., Jacobs, J.M., Lanerolle, L.W.J., Moore, S.K., Schwab,
 672 D.J., Trainer, V.L., Trtanj, J., Turner, E.J., Wood, R., Wynne, T., 2012. Towards operational
 673 forecasts of algal blooms and pathogens, In: S. A. Morain and A. M. Budge (Ed.), *Environmental*
 674 *tracking for public health surveillance*. CRC Press, pp. 345-368.
- 675 Brown, M.B., Forsythe, A.B., 1974. Robust Tests for the Equality of Variances. *J. Am. Stat.*
 676 69(346), 364-367.
- 677 Brownlee, E.F., Olson, R.J., Sosik, H.M., 2016. Microzooplankton community structure
 678 investigated with imaging flow cytometry and automated live-cell staining. *Mar. Ecol. Prog.* 550,
 679 65-81.
- 680 Campbell, L., Olson, R.J., Sosik, H.M., Abraham, A., Henrichs, D.W., Hyatt, C.J., Buskey, E.J.,
 681 2010. First harmful *Dinophysis* (Dinophyceae, Dinophysiales) bloom in the U.S. is revealed by
 682 automated Imaging Flow Cytometry. *J. Phycol.* 46(1), 66-75.
- 683 FDA, 2011. Fish and Fishery Products Hazards and Controls Guidance. Department of Health
 684 and Human Services, Public Health Service, Food and Drug Administration, Center for Food
 685 Safety and Applied Nutrition, Office of Food Safety, p. Appendix 5: FDA and EPA Safety
 686 Levels in Regulations and Guidance.
- 687 García-Altres, M., Casanova, A., Fernández-Tejedor, M., Diogène, J., de la Iglesia, P., 2016.
 688 Bloom of *Dinophysis* spp. dominated by *D. sacculus* and its related diarrhetic shellfish poisoning
 689 (DSP) outbreak in Alfac Bay (Catalonia, NW Mediterranean Sea): Identification of DSP toxins
 690 in phytoplankton, shellfish and passive samplers. *Reg. Stud.* 6, 19-28.

- 691 García-Portela, M., Reguera, B., Sibat, M., Altenburger, A., Rodríguez, F., Hess, P., 2018.
692 Metabolomic Profiles of *Dinophysis acuminata* and *Dinophysis acuta* Using Non-Targeted High-
693 Resolution Mass Spectrometry: Effect of Nutritional Status and Prey. *Mar. Drugs* 16(5), 143.
- 694 Glibert, P.M., Pitcher, G.C., Bernard, S., Li, M., 2018. Advancements and Continuing
695 Challenges of Emerging Technologies and Tools for Detecting Harmful Algal Blooms, Their
696 Antecedent Conditions and Toxins, and Applications in Predictive Models, In: Glibert, P.M.,
697 Berdalet, E., Burford, M.A., Pitcher, G.C., Zhou, M. (Eds.), *Global Ecology and Oceanography*
698 *of Harmful Algal Blooms*. Springer International Publishing, Cham, pp. 339-357.
- 699 Hansen, P.J., Nielsen, L.T., Johnson, M., Berge, T., Flynn, K.J., 2013. Acquired phototrophy in
700 *Mesodinium* and *Dinophysis* – A review of cellular organization, prey selectivity, nutrient uptake
701 and bioenergetics. *Harmful Algae* 28, 126-139.
- 702 Harred, L.B., Campbell, L., 2014. Predicting harmful algal blooms: a case study with *Dinophysis*
703 *ovum* in the Gulf of Mexico. *J. Plankton Res.* 36(6), 1434-1445.
- 704 Hattenrath-Lehmann, T.K., Marcoval, M.A., Berry, D.L., Fire, S., Wang, Z., Morton, S.L.,
705 Gobler, C.J., 2013. The emergence of *Dinophysis acuminata* blooms and DSP toxins in shellfish
706 in New York waters. *Harmful Algae* 26, 33-44.
- 707 Holm, S., 1979. A Simple Sequentially Rejective Multiple Test Procedure. *Scand. J. Stat.* 6(2),
708 65-70.
- 709 Jin, D., Hoagland, P., 2008. The value of harmful algal bloom predictions to the nearshore
710 commercial shellfish fishery in the Gulf of Maine. *Harmful Algae* 7(6), 772-781.
- 711 Kim, M., Nam, S.W., Shin, W., Coats, D.W., Park, M.G., 2012. *Dinophysis caudata*
712 (Dinophyceae) sequesters and retains plastids from the mixotrophic ciliate prey *Mesodinium*
713 *rubrum*. *J. Phycol.* 48(3), 569-579.
- 714 Kudela, R.M., Anderson, C., Ruhl, H., 2021. The California Harmful Algal Bloom Monitoring
715 and Alert Program: A Success Story for Coordinated Ocean Observing. *Oceanogr.* 34(4), 84-85.
- 716 Lindahl, O., Lundve, B., Johansen, M., 2007. Toxicity of *Dinophysis* spp. in relation to
717 population density and environmental conditions on the Swedish west coast. *Harmful Algae* 6(2),
718 218-231.
- 719 Lloyd, J.K., Duchin, J.S., Borchert, J., Quintana, H.F., Robertson, A., 2013. Diarrhetic shellfish
720 poisoning, Washington, USA, 2011. *Emerg. Infect. Dis.* 19(8), 1314.
- 721 McGaraghan, A., Hayashi, K., Daniel, P., Kudela, R.M., 2022. Development and comparison of
722 Imaging FlowCytobot classifiers in coastal California, In: Band-Schmidt, C.J., Rodríguez-
723 Gómez, C.F. (Eds.), *Proceedings of the 19th International Conference on Harmful Algae*, La Paz,
724 B.C.S., Mexico. International Society for the Study of Harmful Algal Blooms, pp. 220-224.
- 725 Moberg, E.A., Sosik, H.M., 2012. Distance maps to estimate cell volume from two-dimensional
726 plankton images. *Limnol. Oceanogr.: Methods* 10(4), 278-288.
- 727 Nagai, S., Nitshitani, G., Tomaru, Y., Sakiyama, S., Kamiyama, T., 2008. Predation by the toxic
728 dinoflagellate *Dinophysis fortii* on the ciliate *Myrionecta rubra* and observation of sequestration
729 of ciliate chloroplasts. *J. Phycol.* 44(4), 909-922.
- 730 NCCOS and US IOOS, 2020. Framework for the National Harmful Algal Bloom Observing
731 Network: A workshop Report. National Centers for Coastal Ocean Science, p. 59.
- 732 Neeley, A., Beaulieu, S., Proctor, C., Cetinić, I., Futrelle, J., Soto Ramos, I., Sosik, H., Devred,
733 E., Karp-Boss, L., Picheral, M., 2021. Standards and practices for reporting plankton and other
734 particle observations from images. 38pp.
- 735 Nielsen, L.T., Krock, B., Hansen, P.J., 2012. Effects of light and food availability on toxin
736 production, growth and photosynthesis in *Dinophysis acuminata*. *Mar. Ecol. Prog.* 471, 37-50.

- 737 Nielsen, L.T., Krock, B., Hansen, P.J., 2013. Production and excretion of okadaic acid,
738 pectenotoxin-2 and a novel dinophysistoxin from the DSP-causing marine dinoflagellate
739 *Dinophysis acuta* – Effects of light, food availability and growth phase. *Harmful Algae* 23, 34-
740 45.
- 741 Oksanen, J., Blanchet, G., Friendly, M., Roeland, K., Legendre, P., McGlinn, D., Minchin, P.,
742 O'Hara, R., Simpson, G., Solymos, P., Stevens, H., Szoecs, E., Wagner, H., 2018. vegan:
743 Community Ecology Package. R package version 2.5-3. [https://CRAN.R-](https://CRAN.R-project.org/package=vegan)
744 [project.org/package=vegan](https://CRAN.R-project.org/package=vegan).
- 745 Olson, R.J., Sosik, H.M., 2007. A submersible imaging-in-flow instrument to analyze nano-and
746 microplankton: Imaging FlowCytobot. *Limnol. Oceanogr.: Methods* 5(6), 195-203.
- 747 Park, M.G., Kim, S., Kim, H.S., Myung, G., Kang, Y.G., Yih, W., 2006. First successful culture
748 of the marine dinoflagellate *Dinophysis acuminata*. *Aquat. Microb. Ecol.* 45(2), 101-106.
- 749 Park, M.G., Park, J.S., Kim, M., Yih, W., 2008. Plastid dynamics during survival of *Dinophysis*
750 *caudata* without its ciliate prey. *J. Phycol.* 44(5), 1154-1163.
- 751 Parkhill, J.-P., Maillet, G., Cullen, J.J., 2001. Fluorescence-based maximal quantum yield for
752 PSII as a diagnostic of nutrient stress. *J. Phycol.* 37(4), 517-529.
- 753 Pizarro, G., Escalera, L., González-Gil, S., Franco, J.M., Reguera, B., 2008. Growth, behaviour
754 and cell toxin quota of *Dinophysis acuta* during a daily cycle. *Mar. Ecol. Prog.* 353, 89-105.
- 755 PSEMP Marine Waters Workgroup, 2017. Puget Sound marine waters: 2016 overview, In: S. K.
756 Moore, R.W., K. Stark, J. Bos, P. Williams, N. Hamel, A. Edwards, C. Krembs, and J. Newton
757 (Ed.).
- 758 Reguera, B., Riobó, P., Rodríguez, F., Díaz, P.A., Pizarro, G., Paz, B., Franco, J.M., Blanco, J.,
759 2014. *Dinophysis* Toxins: Causative Organisms, Distribution and Fate in Shellfish. *Mar. Drugs*
760 12(1), 394-461.
- 761 Reguera, B., Velo-Suárez, L., Raine, R., Park, M.G., 2012. Harmful *Dinophysis* species: A
762 review. *Harmful Algae* 14, 87-106.
- 763 Royston, J.P., 1982. An Extension of Shapiro and Wilk's W Test for Normality to Large
764 Samples. *J. R. Stat. Soc.* 31(2), 115-124.
- 765 Smith, J.L., Tong, M., Kulis, D., Anderson, D.M., 2018. Effect of ciliate strain, size, and
766 nutritional content on the growth and toxicity of mixotrophic *Dinophysis acuminata*. *Harmful*
767 *Algae* 78, 95-105.
- 768 Sosik, H.M., Olson, R.J., 2007. Automated taxonomic classification of phytoplankton sampled
769 with imaging-in-flow cytometry. *Limnol. Oceanogr.: Methods* 5(6), 204-216.
- 770 Trainer, V.L., King, T.L., 2023. SoundToxins: A Research and Monitoring Partnership for
771 Harmful Phytoplankton in Washington State. *Toxins* 15(3), 189.
- 772 Trainer, V.L., Moore, L., Bill, B.D., Adams, N.G., Harrington, N., Borchert, J., da Silva,
773 D.A.M., Eberhart, B.-T.L., 2013. Diarrhetic shellfish toxins and other lipophilic toxins of human
774 health concern in Washington State. *Mar. Drugs* 11(6), 1815-1835.
- 775 Trainer, V.L., Suddleson, M., 2005. Monitoring approaches for early warning of domoic acid
776 events in Washington state. *Oceanogr.* 18(2), 228-237.
- 777 Washington Sea Grant, 2015. Shellfish aquaculture in Washington state. Final report to the
778 Washington State Legislature 84p.
- 779 Willén, E., 1976. A simplified method of phytoplankton counting. *Br. Phycol. J.* 11(3), 265-278.
- 780 Yasumoto, T., Murata, M., Oshima, Y., Sano, M., Matsumoto, G.K., Clardy, J., 1985. Diarrhetic
781 shellfish toxins. *Tetrahedron* 41(6), 1019-1025.
- 782

Figure captions

Figure 1: Map of Puget Sound and inlet showing Budd Inlet with location of the Imaging FlowCytobot (IFCB) deployment. Arrows represent water circulation

Figure 2: *Dinophysis acuminata* abundance detected (A & B), effective volume analyzed (C & D) and total number of particles detected (E & F) by the IFCB when triggering the image acquisition on side scattering (left panel) or fluorescence (right panel) using different combinations of photomultiplier tubes (PMTs) gains (symbols) and thresholds (colors) settings. Side scattering gains tested: 0.3, 0.4, 0.5 and 0.6. Side scattering thresholds tested: 0.16, 0.20 and 0.25. Fluorescence gains tested: 0.6, 0.7, 0.8 and 0.9. Fluorescence thresholds tested: 0.125, 0.14 and 0.16. Horizontal dashed line corresponds to the microscopic count and gray highlight represents Willén (1976)'s error rate

Figure 3: Temporal dynamics of *Mesodinium* spp. abundance, total *Dinophysis* spp. abundance and *Dinophysis* species composition in Budd Inlet measured with the Imaging FlowCytobot (IFCB) by triggering on fluorescence (A) and side scattering (B). Each time point is one syringe sample. For comparison, total *Dinophysis* spp. abundance obtained by conventional microscopy is also represented. (A) and (B) share the same legend. (C) Temporal variations in the level of autofluorescence of *Dinophysis* spp. cells (mean \pm standard deviation) measured by the IFCB (IFCB-autofluorescence) by triggering on fluorescence (white circles) and side scattering (black circles) and percentage of fluorescing *Dinophysis* spp. cells observed by epifluorescence microscopy (white triangles). (D) Biovolume of *Dinophysis* spp. cells (mean \pm standard deviation) measured by the IFCB by triggering on fluorescence and side scattering. Black bars on the x-axis indicate IFCB data gaps. The gray shaded area highlights a period when the IFCB detected *Dinophysis* spp. cells when side scattering was used to trigger the image acquisition while triggering on fluorescence did not

Figure 4: Level of IFCB-autofluorescence vs. biovolume of *Dinophysis acuminata*, *Dinophysis fortii*, *Dinophysis norvegica* and *Dinophysis parva*. Black line represents linear regression

Figure 5: (A) Histogram of *Mesodinium* spp. biovolume during June-July and September. (B) Level of IFCB-autofluorescence vs. biovolume of *Mesodinium* spp.

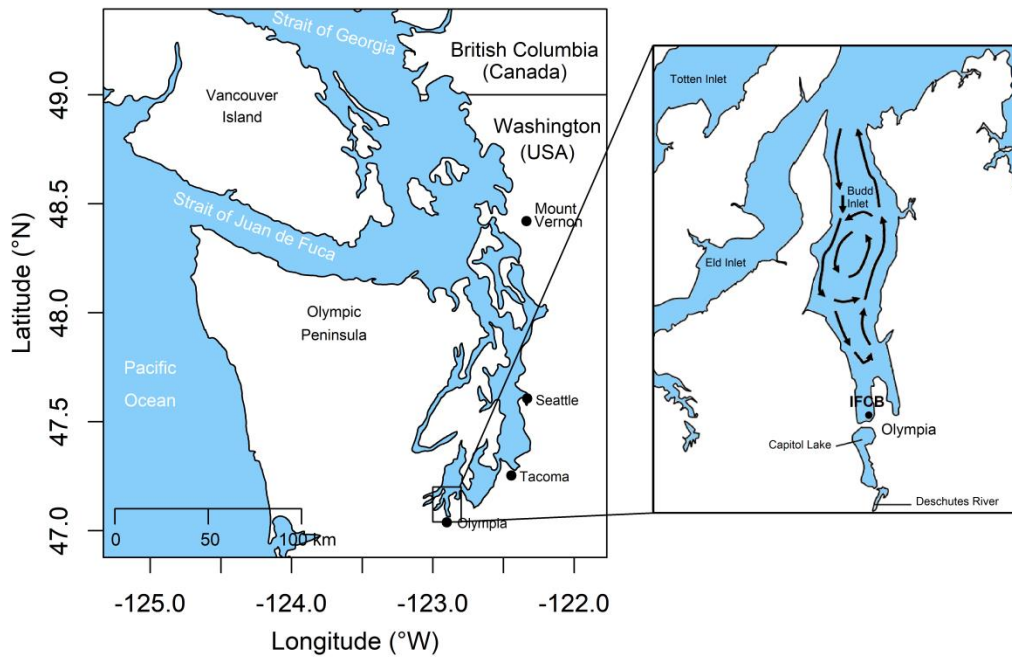


Figure 1: Map of Puget Sound and inlet showing Budd Inlet with location of the Imaging FlowCytobot (IFCB) deployment. Arrows represent water circulation

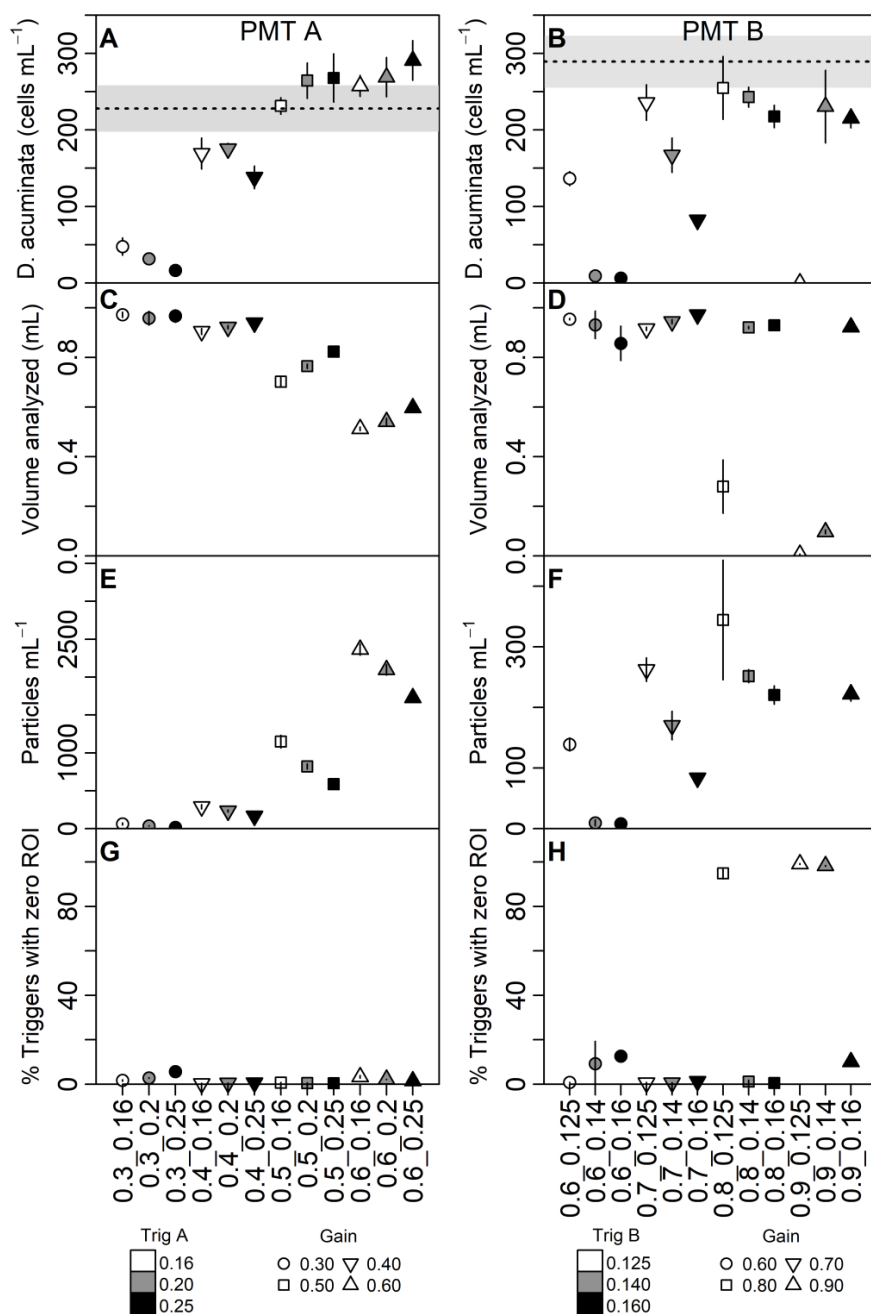


Figure 2: *Dinophysis acuminata* abundance detected (A & B), effective volume analyzed (C & D) and total number of particles detected (E & F) by the IFCB when triggering the image acquisition on side scattering (left panel) or fluorescence (right panel) using different combinations of photomultiplier tubes (PMTs) gains (symbols) and thresholds (colors) settings. Side scattering gains tested: 0.3, 0.4, 0.5 and 0.6. Side scattering thresholds (Trig A) tested: 0.16, 0.20 and 0.25. Fluorescence gains tested: 0.6, 0.7, 0.8 and 0.9. Fluorescence thresholds tested (Trig B): 0.125, 0.14 and 0.16. Horizontal dashed line corresponds to the microscopic count and gray highlight represents Willén (1976)'s error rate. Note scale difference in E and F

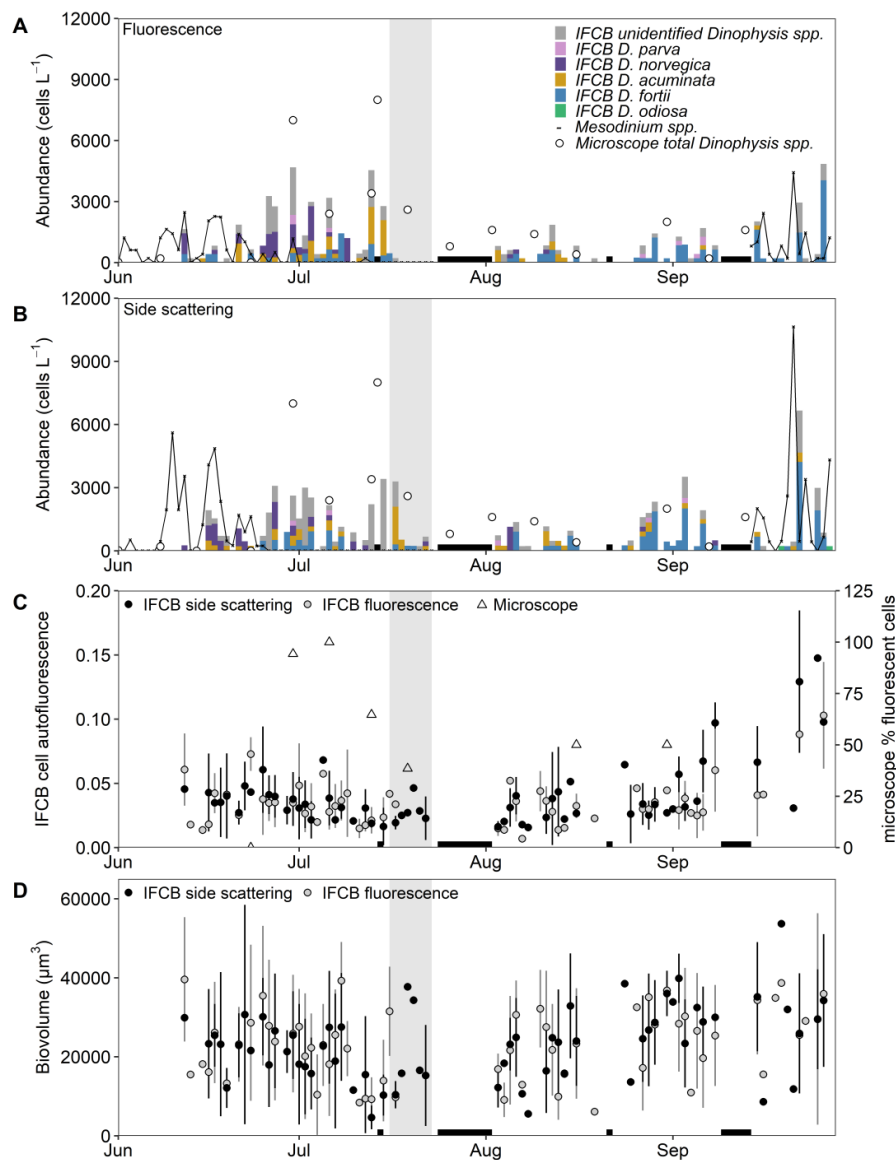


Figure 3: Temporal dynamics of *Mesodinium* spp. abundance, total *Dinophysis* spp. abundance and *Dinophysis* species composition in Budd Inlet measured with the Imaging FlowCytobot (IFCB) by triggering on fluorescence (A) and side scattering (B). Each time point is one syringe sample. For comparison, total *Dinophysis* spp. abundance obtained by conventional microscopy is also represented. (A) and (B) share the same legend. (C) Temporal variations in the level of autofluorescence of *Dinophysis* spp. cells (mean \pm standard deviation) measured by the IFCB (IFCB-autofluorescence) by triggering on fluorescence (white circles) and side scattering (black circles) and percentage of fluorescing *Dinophysis* spp. cells observed by epifluorescence microscopy (white triangles). (D) Biovolume of *Dinophysis* spp. cells (mean \pm standard deviation) measured by the IFCB by triggering on fluorescence and side scattering. Black bars on the x-axis indicate IFCB data gaps. The gray shaded area highlights a period when the IFCB detected *Dinophysis* spp. cells when side scattering was used to trigger the image acquisition while triggering on fluorescence did not

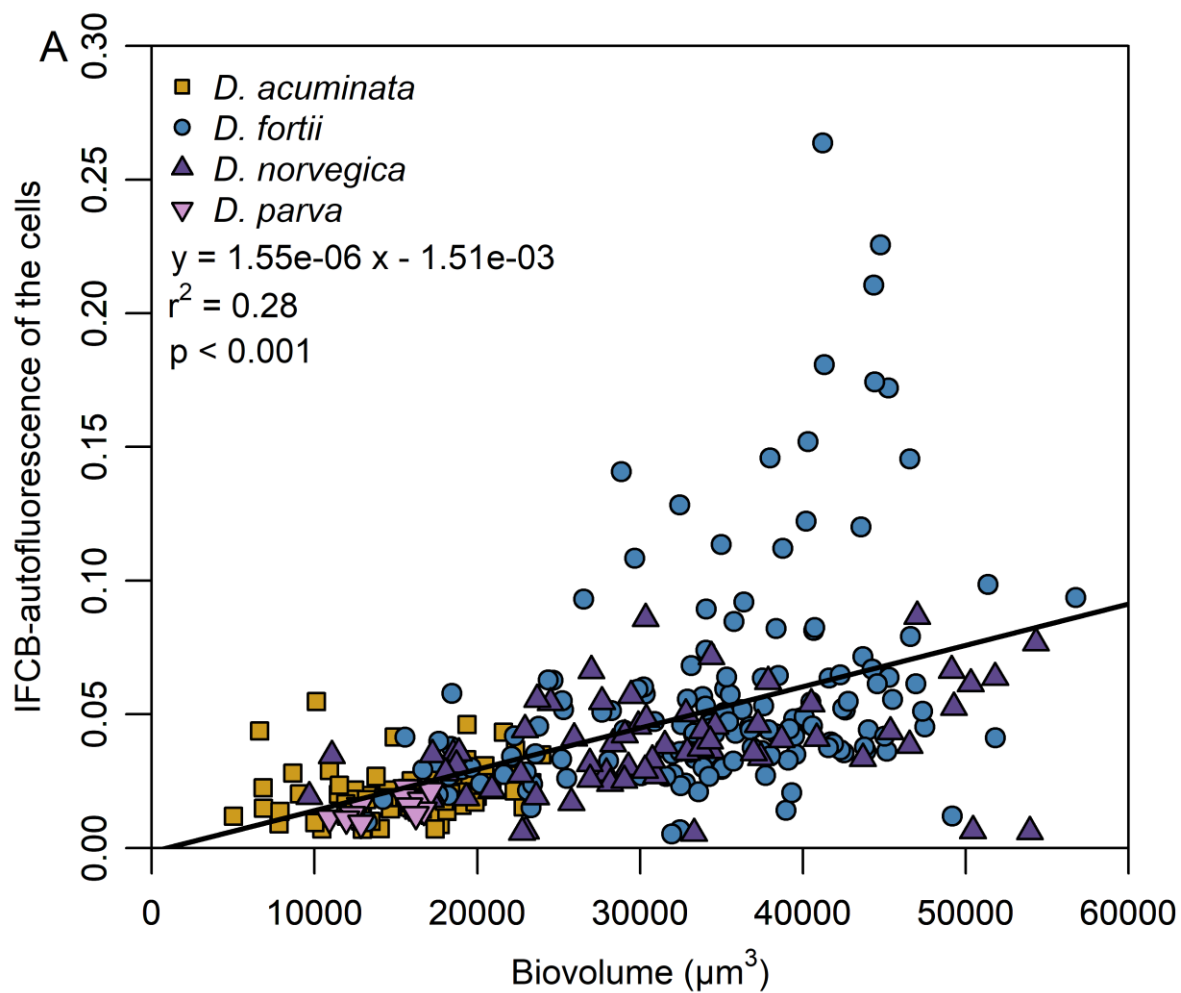


Figure 4: Level of IFCB-autofluorescence vs. biovolume of *Dinophysis acuminata*, *Dinophysis fortii*, *Dinophysis norvegica* and *Dinophysis parva*. Black line represents linear regression

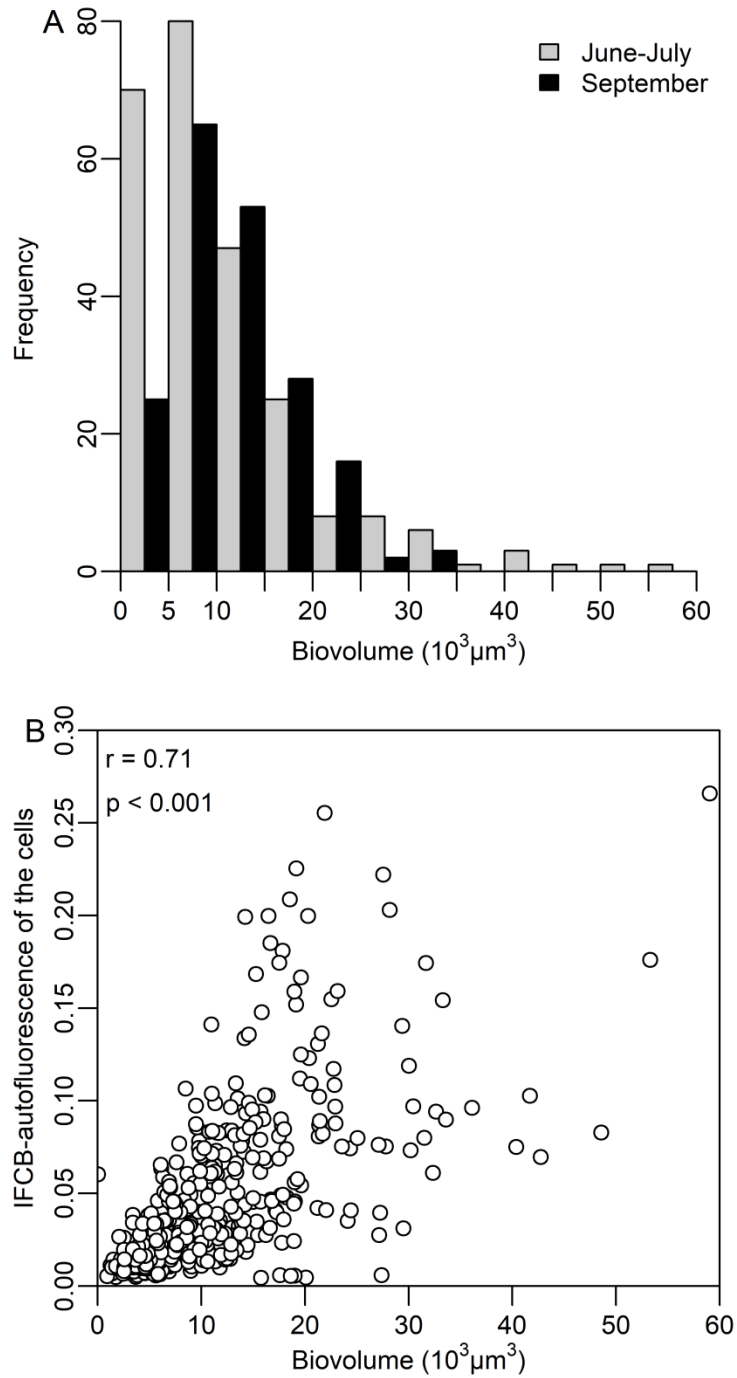


Figure 5: (A) Histogram of *Mesodinium* spp. biovolume during June-July and September. (B) Level of IFCB-autofluorescence vs. biovolume of *Mesodinium* spp.